International Journal of Modern Engineering Research (IJMER)
www.ijmer.com Vol.3, Issue.2, March-April. 2013 pp-1229-1237 ISSN: 2249-6645

Numerical Characterization of the Pores and the Determination of the Point Of Crack Initiation in Some Cast Aluminum Alloys

Durowoju, M.O
Mechanical Engineering Department, Ladoke Akintola University of Technology Ogbomoso, Oyo State Nigeria

Abstract: *Porosity is a major defect in cast aluminum alloys affecting in particular, the fatigue strength. In this work, fractal analysis of the pores in the microstructure of cast aluminum alloys were done to provide information linking their composition and processing to the crack initiation.*

Two cast alloys: Al – 20%wtSi and Al – 20%wtCu, were used and the types of pores were studied in the as-cast samples. The shapes of the pores along with the percentage porosity in each of the microstructures were also evaluated. The Multi-Stage Random Sampling (MRS) and Spatial Point Pattern (SPP) Methods were used to determine the distribution of the pores and the point of crack initiation.

Fractal analysis showed that all the pores were shrinkage pores with $\beta<0.3$ and D approaching 2. The MRS and SPP methods revealed that crack initiation for eventual failure will start in the worst pore found in the lower right region of as-cast Al-20%wtSi because it has the value of D= 1.2846 and lowest sphericity β =0.0011.

This work has shown the effectiveness of using the fractal analysis, the MRS and the SPP methods for the characterization of the pores in the microstructure of cast aluminium alloys.

Keywords: *Fractal Analysis, Pores, MRS and SPP methods*

I. Introduction

For alloys and composite materials containing regular microstructures, a prediction of mechanical properties can be made by a quantitative measurement of features such as grain size, particle size, and spacing. This however is not the case where an irregular microstructure is involved because of the difficulty in the numerical characterization of the structure. For irregular microstructures, the application of fractal geometry offers a method by which both the individual particle shape and the mode of the distribution of the particles can be fully described in a numerical manner (1).

A Study carried out to evaluate the dependence of surface fractal dimension of Al_2O_3-SiO_2 composite membranes on chemical composition and sintering temperature (2) has shown that all composite membranes have rough surfaces with fractal dimensions ranging from 2 to 3. As SiO_2 content increases and sintering temperature rises from 200 to 600^0C, the fractal dimension increases. However, at 800^oC, the surface fractal dimension decreases. The computer aided stereo matching method on metals and ceramics was used to reconstruct the three-dimensional images of fracture surfaces formed by different mechanisms (3). An extensive experimental investigation of the scaling properties of fracture surfaces in heterogeneous materials was done (4). It was discovered that all the surfaces of the materials (silica glass, aluminum alloy, mortar and wood) investigated far from crack initiation point, are self –affine. In addition, it was observed that the Hurst exponent measured along the crack direction is found to be different from the one measured along the propagation direction. Furthermore, ductile fracture surface had the larger fractal dimension compared with the brittle type fracture surface.
The measurement of the porosity in aluminum cast alloys using fractal analysis was done (5). They observed that fractal analysis can be applied to the porosity measurement to describe the shapes of the pores in the aluminum silicon cast alloys using two dimensionless parameters, roughness, D and sphericity, β.

Spatial data analysis was used to study the distribution of micro porosity in 7050-T7451 aluminum plate alloys (6) and it was observed that the micro porosity was not randomly distributed throughout the sample. Similarly, another study on the distribution of micro porosity in an A356 aluminum alloy plate casting was done (7). From the study, it was concluded that the porosity was not randomly distributed but clustered, and that the clustering tendency was relatively constant throughout the casting. The patterns observed in the porosity distribution maps shown in Figure 1 was used to categorize the pores into random, regular, clustered, and clustered with random background (8). In the present work, the intention is to use the fractal analysis to characterize the pores in Al – 20%wtSi, and Al – 20%wtCu cast aluminum alloys and to identify the points of crack initiation using MRS and SPP methods.

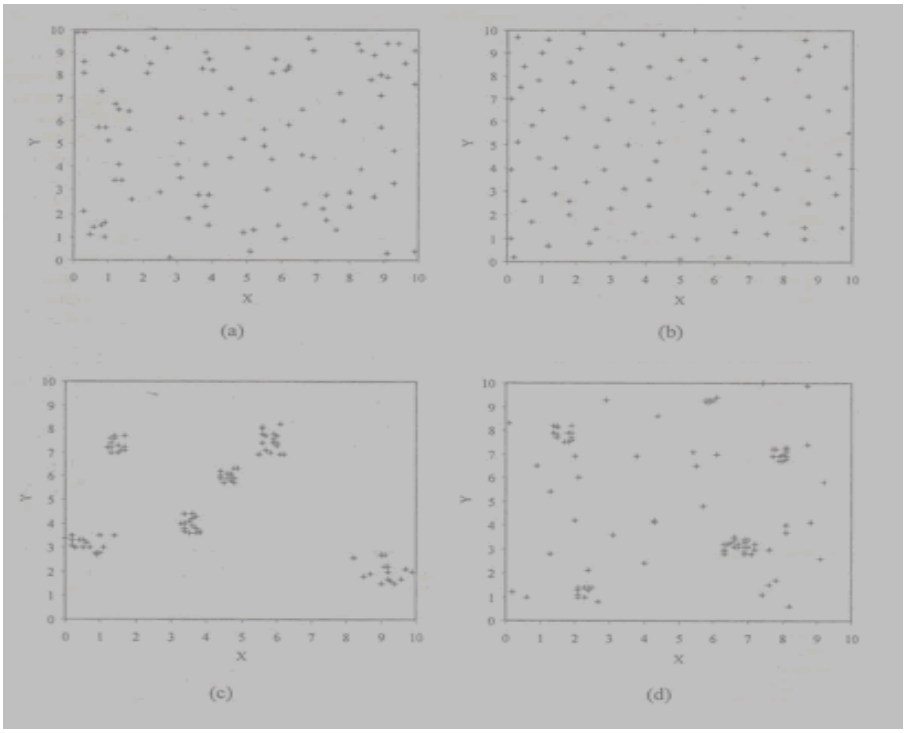

Fig. 1: The four common types of spatial point patterns (a) random, (b) regular, (c) clustered, (d) clustered superimposed on random background**.**

II. Materials and Methods

1kg (80% by proportion) of commercial aluminum (99.7% pure, by weight) and 250g each (20% by proportion) of Si and Cu, obtained from the Federal Institute of Industrial Research Oshodi (FIIRO), were prepared for the casting. Due to closeness in melting temperatures, pot A which contains Al+Si, with its contents was lowered into the furnace and the mixture melted.

In pot B, the alloying element Cu was first charged in the pot because of its high melting point of about 1108^{o}C. When the melting point was attained, the base metal Aluminum with melting point of 660^{o}C was added.

The molten alloys were poured into the prepared mould after cooling for three minutes (to avoid splashing). The two resulting cast samples in rod forms were removed from the mould after three hours (to allow for effective cooling).

Application of fractals

Fractal geometry was developed (10). Its principle is universal in any measurement and has been previously used to numerically describe complex microstructures including graphite flakes and nodules (1, 11, 12, 13, and 14). The Mathematical basis for measuring chaotic objects with the power law modified is adopted in this work. The basic equation is as follows:

$$P = P_E \delta^{D-1} \qquad \text{Eq 1}$$

$$\left(1 < D < 2 \text{ and } \delta_m < \delta < \delta_M\right) \qquad \text{Eq 1}$$

Where P_E is the measured perimeter, P is the true perimeter, δ is the yardstick,

From this expression, it can be deduced that the true perimeter is actually a function of the yardstick for measurement. The smaller the yardstick used, the more accurate the measurement. The fractal dimension, D, therefore describes the complexity of the contour of an object. It can be more practically called its roughness (5).

When $\delta < \delta_m$, the measurement is not sensitive to the yardstick chosen, therefore giving a smaller value of the slope, while when $\delta > \delta_M$, the size of the yardstick exceeds that of the individual feature being measured so that the measurement loses meaning because the object falls below the resolution limit of the yardstick used for measurement (1). Sphericity, β, another dimensionless number, is used together with the fractal dimension, D; to describe the shape of the pores formed (5). It can be expressed as

$$\beta = 4\pi A_T / P^2 \qquad \text{Eq 2}$$

$$\left(0 < \beta < 1 \text{ and } 1 < D < 2\right)$$

Substituting equation (Eq 1) in (Eq 2) gives

$$\beta = \left(4\pi A_T / P_E^2\right)\delta^{2(1-D)} \qquad \text{Eq 3}$$

$$\left(0 < \beta < 1 \text{ and } 1 < D < 2\right)$$

Where A_T is the total pore area
When $\beta = 1$ and $D = 1$, a perfect circular shape is formed by the pore in the microstructure.
As β decreases, the shapes become more elongated showing a departure from perfect sphere.
The locations of $1 < D < 2$ represent less regular shapes.

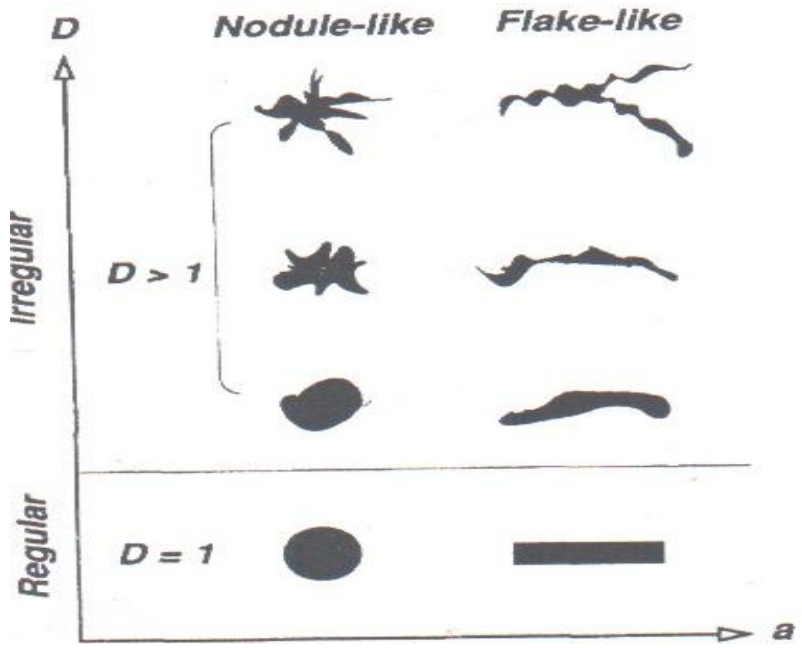

Fig. 2: Illustration of development of irregular shapes based upon Euclidean circle or rectangle. All the shapes have the same area. Source: Lu and Hellawell, (1994) (1)

Where **a** is the Shape Factor.

In Figure 2 the more complex shapes for each individual island present increasing ranges of local curvature and the fractal dimension, D, increases. By definition, the shape factors also change, as they do for Euclidean shapes, but not in a readily calculated manner, because the shape factor (**a)** is now a function of D.

Area of a pixel or yardstick = L x B
Area of the total pore A_T = Area of yardstick x Number of yardsticks
To calculate the perimeter *P* of the pore, the Slit Island Method (SIM)
(15) Introduced by Mandelbrot (1983) was used. It is expressed as:

$$\log_e P = 0.5 D \log_e A_T \qquad \text{Eq 4}$$

$$\log_e P = \log_e A_T^{D/2}$$

$$P = A_T^{D/2}$$

The Computer Program

Using the equations (Eq 1)-(Eq 4), an interactive Matlab program was developed to obtain the numerical values of the fractal dimension *D* and the sphericity β. To develop the program the box counting method was used with a counter incorporated into the program and the small boxes or pixels occupied by the pore outlines are counted. In all four pixels (2x2pixels, 4x4pixels, 8x8pixels and 16x16pixels) and four grid sizes (200x200, 100x100, 50x50 and 25x25) were selected. The selections were made for better resolution and to obtain accurate values. A flowchart showing the various stages and the subroutines in the computer program was drawn as shown in Fig.3.

MRS and SPP Methods.

The first stage involves the division of the microstructures into four quadrants (lower left, upper left, lower right, and upper right) as shown in Figure 4. The second stage is the random selection of two pores from each quadrant while the third stage is the purposive selection (purposive sampling) of the "worst" and the "best" pores from the eight pores selected from each microstructure. The fourth stage is the categorization of the porosity distribution map into random, regular, clustered, and clustered with random background. Fifth stage is the discrimination between the shrinkage and the gaseous pores. In this stage, the patterns described in stage four are associated with different types of porosity.

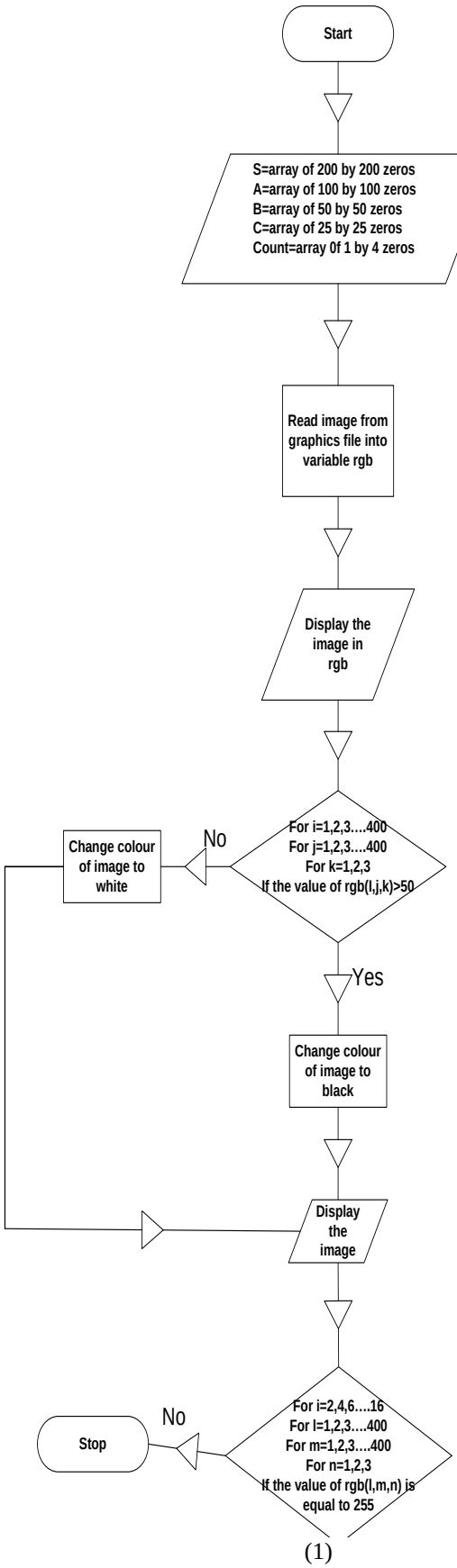
Start
S=array of 200 by 200 zeros
A=array of 100 by 100 zeros
B=array of 50 by 50 zeros
C=array of 25 by 25 zeros
Count=array 0f 1 by 4 zeros
Read image from graphics file into variable rgb
Display the image in rgb
For i=1,2,3....400
For j=1,2,3....400
For k=1,2,3
If the value of rgb(I,j,k)>50
No
Change colour of image to white
Yes
Change colour of image to black
Display the image
For i=2,4,6....16
For I=1,2,3....400
For m=1,2,3....400
For n=1,2,3
If the value of rgb(I,m,n) is equal to 255
No
Stop

(1)

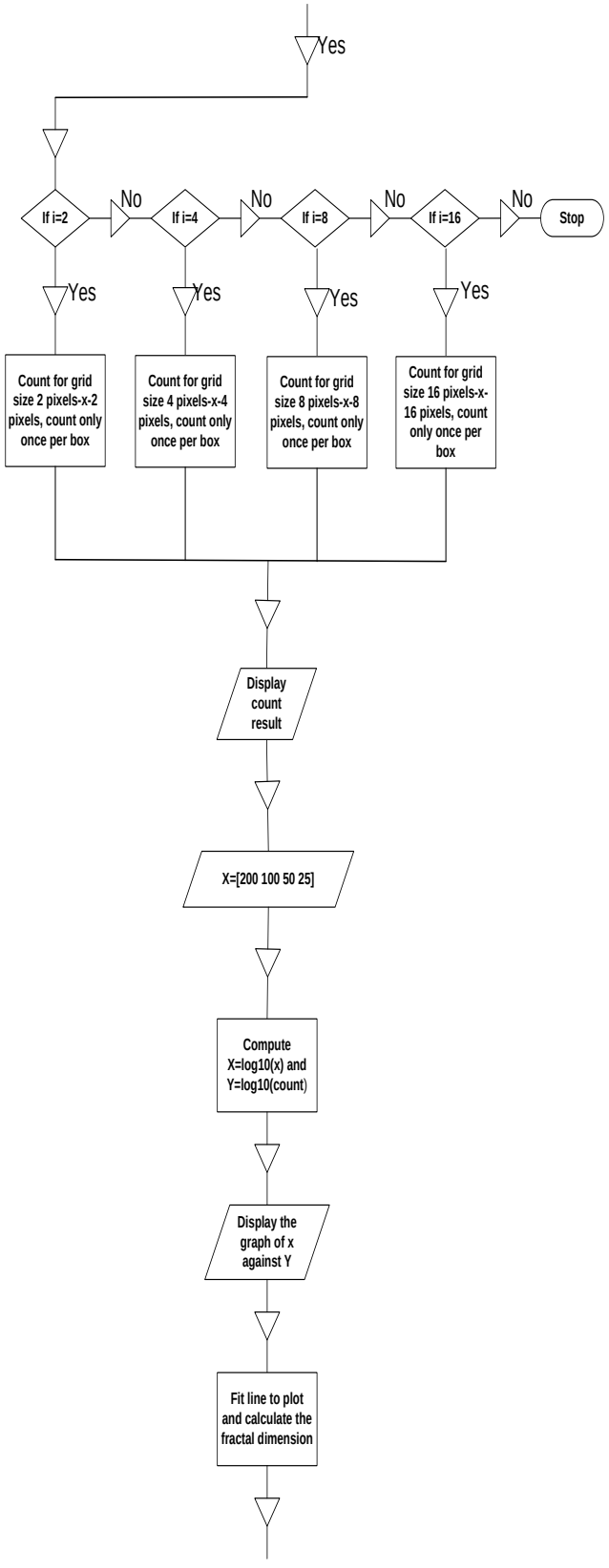
Yes
If i=2
No
If i=4
No
If i=8
No
If i=16
No
Stop
Yes
Yes
Yes
Yes
Count for grid size 2 pixels-x-2 pixels, count only once per box
Count for grid size 4 pixels-x-4 pixels, count only once per box
Count for grid size 8 pixels-x-8 pixels, count only once per box
Count for grid size 16 pixels-x-16 pixels, count only once per box
Display count result
X=[200 100 50 25]
Compute X=log10(x) and Y=log10(count)
Display the graph of x against Y
Fit line to plot and calculate the fractal dimension

(2)

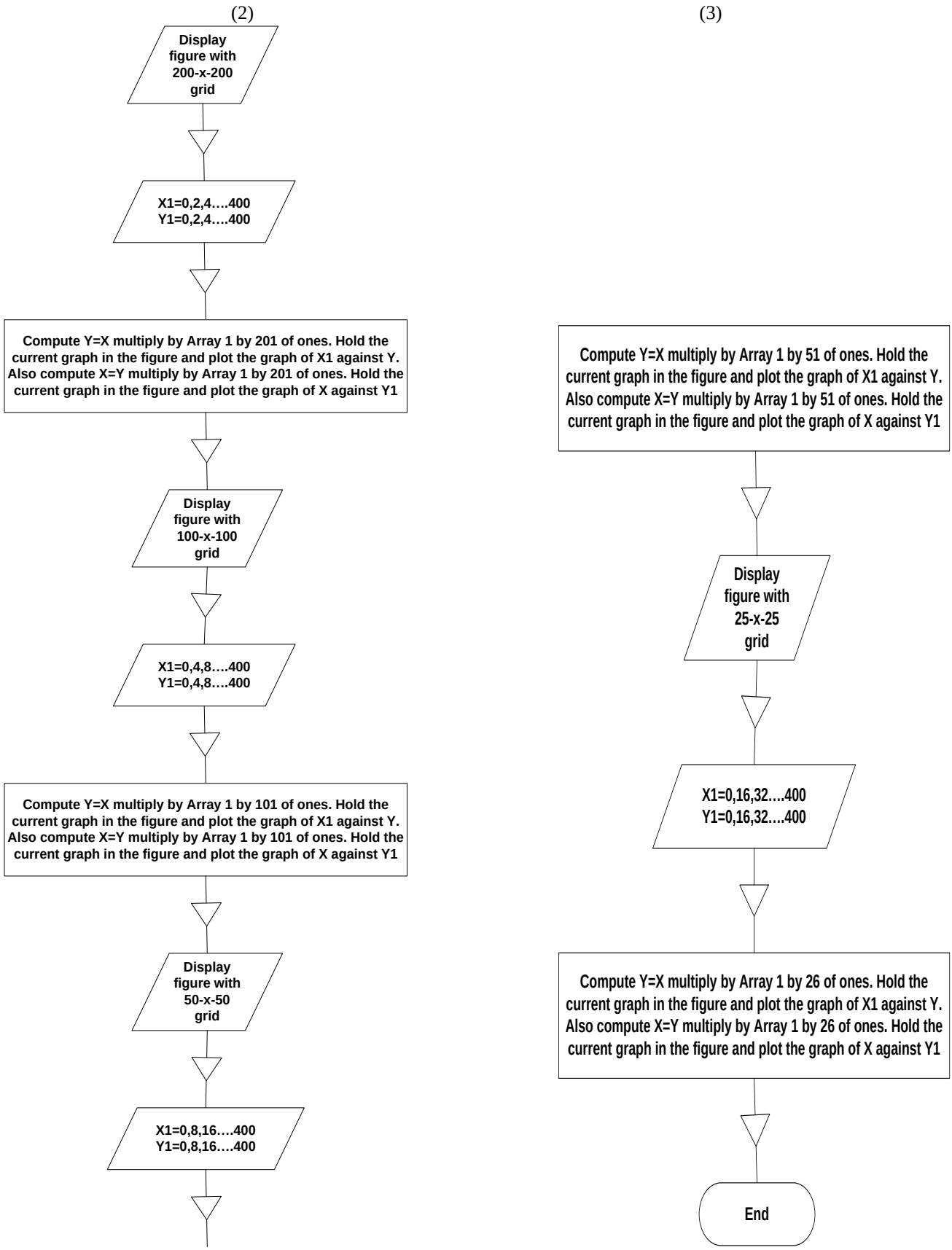

Fig.3: Flow chart of the computer program

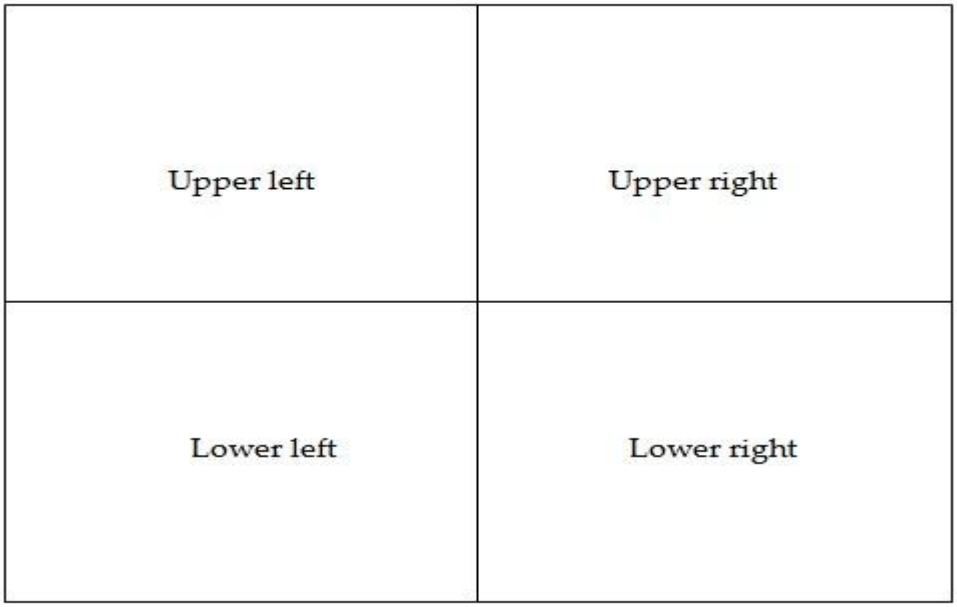

Fig. 4: The Multi-Stage Random Sampling Method of Dividing a Microstructure into four Quadrants.

III. Results and Discussions

Figure 5 shows the microstructures of the two alloy samples used in this work and the isolation of the pores in these samples. The shapes of the pores observed in the microstructures are summarized in Table 1 while the samples of the pores in the microstructures are shown in Figure 6. The pores are all-irregular in shape and are either nodule-like or flake-like.

It was observed that, for the as-cast samples, the predominant pores in Al-20%wtCu are the nodule-like pores while the flake-like pores dominate in Al-20%wtSi (see Table 1). The formation of the nodule-like or flake-like shape is due to the nucleation and growth kinetics usually compounded by composition variations and the concentration of elements such as copper, zinc, magnesium, and silicon in the samples.

Table 1: Shapes of the pores and the dominating shapes in the microstructures of as-cast samples

Cast Samples	Shapes of the Pores	
	Major Pores	Minor Pores
Al-20%wtCu	Nodule-Like	Flake-like
Al-20%wtSi	Flake-like	Nodule-Like

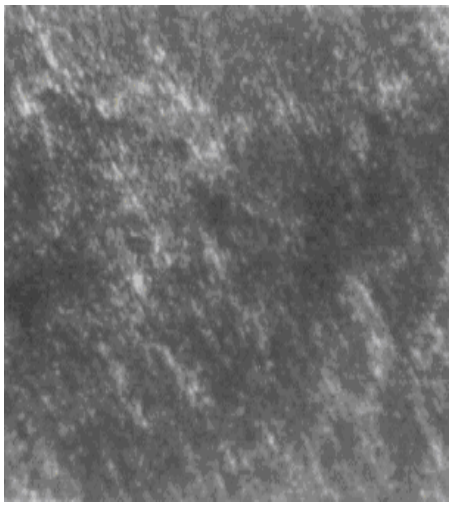

a: Al-20%wtCu

b:Isolation of the pores in Al-20%Cu

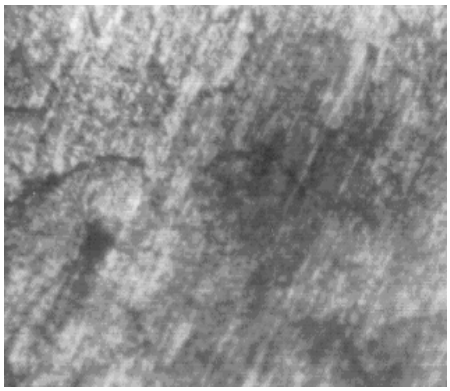

c: Al-20%wtSi

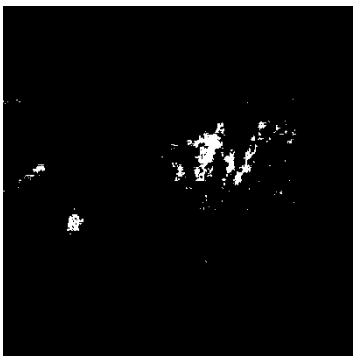

d: Isolation of the pores in Al-20%Si

Fig. 5: Microstructures of as-cast aluminum alloys

Legend:
Dark spot … pore
Grey spot … intermetallic particle
White spot…... Al-matrix

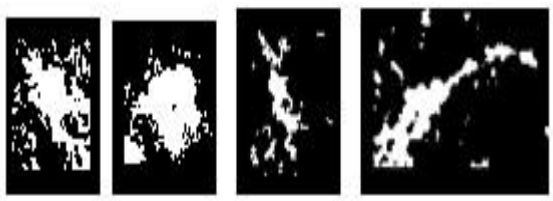

Fig. 6: Samples of pores from the microstructures

PERCENTAGE POROSITY

The percentage porosity, ratio of the pore area to the total area, in each of the as-cast sample, is illustrated in Table 2. It was observed that for the as-cast samples, Al-20%wtSi has the highest number with percentage porosity of 9.92% while Al-20%wtCu has the lowest number with percentage porosity of 4.48%. This is because of the different composition and concentration of the alloying elements. The large atomic radius of Copper compared to that of Silicon ease the formation of pores in the interstitial spaces created in Al-20%wtSi. Copper has atomic radius of 1.57Å, while Silicon has 1.46Å.

Table 2: Percentage Porosity

	As-Cast
Al-20%wtCu	4.48%
Al-20%wtSi	9.92%

Fractal analysis, MRS and SPP Methods

Table 3 presents the fractal dimension, sphericity and pore location for as-cast Al-20%wtCu alloy. The porosity distribution map (Figure 7) gives the "best" of the pores observed as the pore with D =1.0028 and β = 0.0459 while the "worst" of the pores is that with D =1.0678 and β = 0.0135 corresponding to pores numbers N8 and N7 respectively. Using spatial point data analysis, the pores in Figure 7 have regular spatial point pattern and the porosity distribution map represents gas porosity because gas pores are found at a distance from their immediate neighbours due to depletion of hydrogen gas in the area surrounding each pore.

Table 3: Values of fractal dimension D, and sphericity □, for (Al-20%wtCu) As- Cast Alloys

S/n	Alloys	Fractal Dimension D	Sphericity □	Pore Location
N1	Al-20%wtCu1	1.0462	0.0242	Upper right
N2	Al-20%wtCu2	1.0218	0.0266	Upper right
N3	Al-20%wtCu3	1.0966	0.0827	Upper left
N4	Al-20%wtCu4	1.0346	0.0228	Upper left
N5	Al-20%wtCu5	1.0080	0.0195	Lower left
N6	Al-20%wtCu6	1.0574	0.0250	Lower left
N7	Al-20%wtCu7	1.0676	0.0135	Lower right
N8	Al-20%wtCu8	1.0028	0.0459	Lower right

It can be deduced from Table 4 (for Al-20%wtSi alloy as-cast) and the porosity distribution map (Figure 8), that the "best" of the pores observed is the pore with D =1.0847 and β = 0.0579 while the "worst" of the pores is that with D = 1.2846 and β = 0.0011 corresponding to pores numbers N6 and N2 respectively. Figure 8 also has pores with random spatial point pattern because of the closeness of the pores to their immediate neighbours. The porosity distribution map therefore represents gas porosity. The implication of having only regular and random spatial point patterns, representing gas porosity in as-cast samples, is that the pores cannot easily link the nearest neighbour therefore making crack initiation difficult. Another implication is that if failure of the material will occur it will start at the locations with the worst pore shapes.

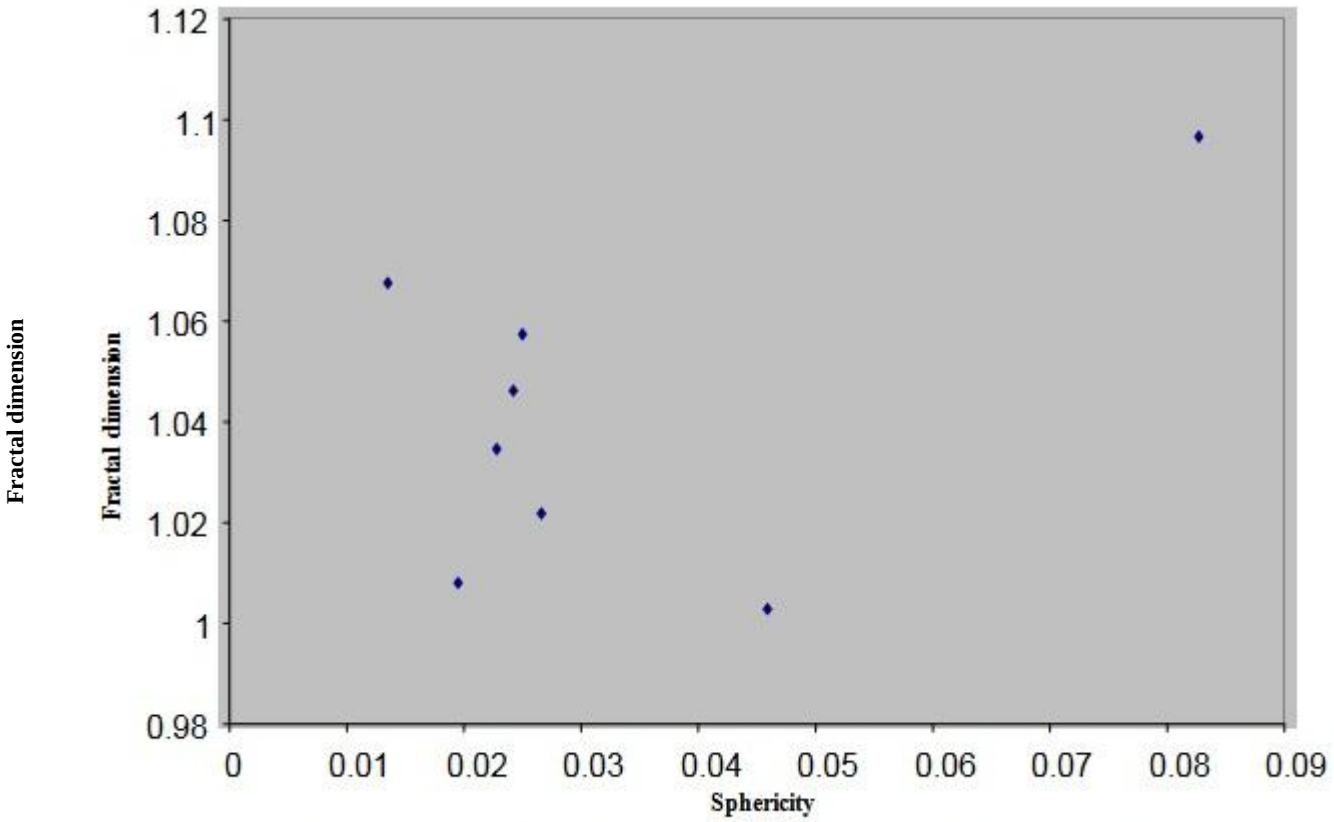

Fig. 7: Porosity distribution map for Al-20%wtCu As-cast Sample

Table 4: Values of fractal dimension D, and sphericity □, for (Al-20%wtSi) As-cast Alloys

S/N	Alloys	Fractal Dimension D	Sphericity □	Pore Location
N1	Al-20%wtSi1	1.0510	0.0348	Upper right
N2	Al-20%wtSi2	1.2846	0.0011	Upper right
N3	Al-20%wtSi3	1.1087	0.0074	Upper left
N4	Al-20%wtSi4	1.1278	0.0104	Upper left
N5	Al-20%wtSi5	1.1633	0.0057	Lower left
N6	Al-20%wtSi6	1.0847	0.0579	Lower right
N7	Al-20%wtSi7	1.0440	0.0114	Lower right
N8	Al-20%wtSi8	1.1253	0.0126	Lower left

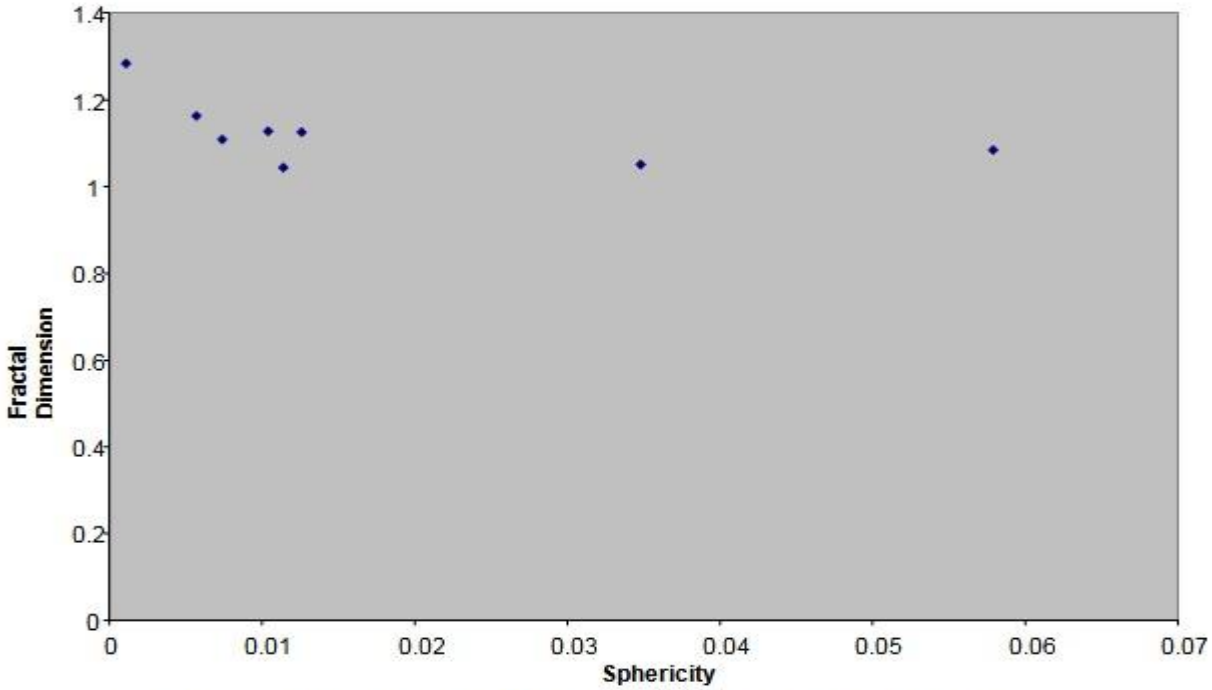

Fig.8: Porosity Distribution Map for Al-20%wtSi As-cast Sample

IV. Conclusions

- The noodle-like pores are the major pores in as-cast Al-20%wtCu while the flake-like pores are the major pores in Al-20%wtSi.
- The MRS and SPP methods revealed that if crack initiation will occur it will start in:
- Lower right region of as-cast Al-20%wtCu because it contains the "worst" pore shape with D = 1.0676 and β = 0.0135.
- Upper right region of as-cast Al-20%wtSi because it contains the "worst" pore shape with D = 1.2846 and β = 0.0011.

References

[1] Lu, S.Z and Hellawell, A. (1994) "An Application of Fractal Geometry to Complex Microstructures: Numerical Characterization of Graphite in Cast Irons", Acta Metall., Vol.42 pp. 4035-4047.
[2] Wei, Q., and Wang, D. (2003); "Pore Surface Fractal Dimension of Sol-Gel-Derived Al_2O_3-SiO_2 Membranes" Material Letters, Vol.57, pp.2015-2020.
[3] Tanaka, M.,Kimura, Y., Kayama, A., Kato, R., and Taguchi, J. (2004) " Fractal Analysis of Three-Dimensional Fracture Surfaces in Metals and Ceramics" ISIJ International, Vol. 44 No. 7 pp1250-1257.
[4] Ponson, L., Bonamy D., Auradon H., Mourot G., Morel S., Bouchaud E., Guillot C., and Hulin J.P.(2006)"Anisotropic Self – Affine Properties of Experimental Fracture Surfaces" International Journal of Fracture Vol.140 No.1-4 pp .27-37.
[5] Huang, Y. J., and Lu S.Z. (2002) "A Measurement of The Porosity in Aluminum cast Alloys Using Fractal Analysis" Proceeding of 2nd International Aluminum Casting Technology Symposium, ASME, Houston U.S.A.
[6] Zhang, J., Przystupa, M. A. and Luevano, A. J. (1998); "Characterization of Pore and Constituent Particle Populations in 7050-T7451 aluminum Plate Alloys" Metallurgical Transaction Vol.29A pp. 727-737.
[7] Tewari, A., Dighe, M., and Gokhale, A.M. (1998) "Quantitative Characterization of Spatial Arrangement of Micro pores in Cast Microstructures" Material Characterization.Vol.40 pp119-132.
[8] Anson, J. P., and Gruzleski, J. E. (1999) "The Quantitative Discrimination between Shrinkage and Gas Porosity Using Spatial Data Analysis" Materials Characterization .Vol.43 pp 319-335.
[9] Mandelbrot, B., B. (1983) "The Fractal Geometry of Nature", Freeman Publishers, London.
[10] Lu, S.Z and Hellawell, A. (1995[a]) "Fractal Analysis of Complex Microstructures in Materials", Proc. of MC95 International Metallographic Conference, May 10-12, Colmar, France, ASM pp. 119.
[11] Lu, S.Z and Hellawell, A. (1995[b]) "Modification of Aluminium-Silicon Alloys: Microstructural Change, Thermal Analysis and Mechanism", Journal of Materials, Vol.47 pp. 38-40.
[12] Lu, S.Z and Hellawell, A. (1995[c]); "Using Fractal Analysis to Describe Irregular Microstructures", Journal of Materials, Vol.47 pp. 14-17.
[13] Lu, S.Z and Hellawell, A. (1999); "A Fractal Method of Modularity Measurement in Ductile Iron", American Foundry Society Transaction, Vol. 107 No. 99-195, pp. 757-162
[14] Bigeralle, M. and Iost, A. (2006) "Perimeter Analysis of the Von Koch Island, Application to the Evolution of Grain Boundaries during Heating" Journal of Material Science. Vol. 41, pp. 2509-2516.